Retrieving Exoplanet Atmospheres Using Planetary Infrared Excess: Prospects for the Night Side of WASP-43 b and Other Hot Jupiters

Jacob Lustig-Yaeger[1,2] , Kevin B. Stevenson[1] , L. C. Mayorga[1] , Kristin Showalter Sotzen[1,3] , Erin M. May[1] ,
Noam R. Izenberg[1] , and Kathleen Mandt[1]
[1] Johns Hopkins University Applied Physics Laboratory, Laurel, MD 20723, USA; Jacob.Lustig-Yaeger@jhuapl.edu
[2] NASA NExSS Virtual Planetary Laboratory, Box 351580, University of Washington, Seattle, Washington 98195, USA
[3] Johns Hopkins University, 3400 N. Charles Street, Baltimore, MD 21218, USA

Abstract

To increase the sample size of future atmospheric characterization efforts, we build on the planetary infrared excess (PIE) technique that has been proposed as a means to detect and characterize the thermal spectra of transiting and non-transiting exoplanets using sufficiently broad wavelength coverage to uniquely constrain the stellar and planetary spectral components from spatially unresolved observations. We performed simultaneous retrievals of stellar and planetary spectra for the archetypal planet WASP-43b in its original configuration and a non-transiting configuration to determine the efficacy of the PIE technique for characterizing the planet's night-side atmospheric thermal structure and composition using typical out-of-transit JWST observations. We found that using PIE with JWST should enable the stellar and planetary spectra to be disentangled with no degeneracies seen between the two flux sources, thus allowing robust constraints on the planet's night-side thermal structure and water abundance to be retrieved. The broad wavelength coverage achieved by combining spectra from NIRISS, NIRSpec, and MIRI enables PIE retrievals that are within 10% of the precision attained using traditional secondary eclipse measurements, although mid-IR observations with MIRI alone may face up to $3.5\times$ lower precision on the planet's irradiation temperature. For non-transiting planets with unconstrained radius priors, we were able to identify and break the degeneracy between planet radius and irradiation temperature using data that resolved the peak of both the stellar and planetary spectra, thus potentially increasing the number of planets amenable to atmospheric characterization with JWST and other future mission concepts.

Unified Astronomy Thesaurus concepts: Exoplanet atmospheres (487); Exoplanet atmospheric composition (2021); Astronomical methods (1043); Infrared excess (788)

1. Introduction

While transiting planets offer a powerful means to characterize their atmospheres using transit and eclipse spectroscopy, most exoplanets do not transit their host stars as seen from Earth. Similarly, the study of directly imaged exoplanets is currently limited to the youngest, hottest planets at wide separations. As a result, new observational, technological, or theoretical advances that can separate planets from stars are required to enable the atmospheric study of the large population of non-transiting exoplanets orbiting main-sequence stars.

Transiting exoplanets have a reference point *in time* (secondary eclipse) during which the planetary flux is blocked, allowing the stellar and planetary flux to be separated using *temporally resolved* measurements (i.e., time-series observations). Directly imaged exoplanets can be observed with a coronagraph or starshade so that the planet's flux can be *spatially resolved* from that of the host star. Recently, Stevenson (2020; henceforth S20) proposed that the sufficiently broad wavelength coverage provided by the James Webb Space Telescope (JWST; Gardner et al. 2006; Beichman et al. 2014; Kalirai 2018) will allow the planet and star to be *spectrally resolved*. By leveraging the fact that planets and stars of significantly different temperature have separable spectral energy distributions (SEDs), it is possible to fit the two flux sources simultaneously and thereby recover the planetary infrared excess (PIE).

S20 demonstrated that the PIE technique could be used to simultaneously infer the radius and brightness temperature of non-

transiting exoplanets by acquiring simultaneous, broad wavelength spectra, and they discuss how additional planet atmospheric characteristics (such as composition and thermal structure) could be retrieved. S20 also presented several potentially viable applications of the PIE technique, including efficiently studying atmospheric dynamics by obtaining sparsely sampled phase-curve observations, measuring night-side temperatures with transit observations, constraining the radii of directly imaged planets, and searching for biosignatures in planets orbiting the nearest M-dwarf stars. Of these applications, measuring the planet's night-side temperature will be the most straightforward to validate with JWST.

Arcangeli et al. (2021) recently applied a similar approach to the PIE technique using sparsely sampled phase-curve observations of WASP-12b from the Hubble Space Telescope's WFC3 instrument. Using the measured stellar spectrum in eclipse, they placed constraints on the planet's relative spectrum (up to an additive constant) at quadrature phase and, by fitting the slope of the emission spectrum, were able to estimate WASP-12b's brightness temperature. Attempts to repeat this experiment for the planet's night-side using out-of-transit data were unsuccessful due to a significant change in the position of the spectrum on the detector that led to relatively large systematics. Due to JWST's stable location near L2, its pointing repeatability is expected to be significantly better than that of HST (which orbits the Earth; Stevenson & Fowler 2019).

Based on the novel results from Arcangeli et al. (2021), it is clear that the PIE technique offers an invaluable opportunity to

study both transiting and non-transiting thermally bright exoplanets. The transit probability for a hot Jupiter orbiting a Sun-like star is ~10%, thus for every HD 209458b or HD 189733b-like transiting planet, there are 10 times as many non-transiting exoplanets orbiting similarly bright stars. However, before pointing JWST at the nearest known non-transiting hot Jupiter, numerous potential obstacles must be considered in order to demonstrate that the method is not simply *PIE in the sky*. In this paper, we confront the following questions regarding the efficacy of the PIE technique for studying the night side of the hot Jupiter WASP-43b with JWST:

1. Can a planet's atmospheric thermal structure and composition be retrieved using the PIE technique?
2. How degenerate are the stellar and planetary parameters in simultaneous fits to an unresolved spectrum?
3. What are the optimal JWST instruments and exposure times for PIE observations?
4. What is the prospect for PIE on non-transiting exoplanets?
5. What impact does exozodiacal dust have on the retrieved parameters?

In Section 2, we detail novel modifications to a standard exoplanet atmospheric retrieval framework to enable PIE retrievals. In Section 3, we present retrieval results using the PIE technique for WASP-43b with JWST, touching on the sensitivity to wavelength range and exposure time for transiting and non-transiting exoplanets. In Section 4, we discuss our findings in the broader context of the field and conclude with a roadmap for the continued maturity of the PIE technique for exoplanet characterization.

2. Methods

2.1. Retrieval Model

We developed a modified version of the CaltecH Inverse ModEling and Retrieval Algorithms (CHIMERA) code (Line et al. 2013b, 2014b) to operate using the PIE technique. CHIMERA is a flexible, open-source, and well-established retrieval framework used to infer the atmospheric composition of exoplanets from emission and transmission spectroscopy measurements in the optical to mid-infrared for a wide variety of planet types (terrestrial to ultra-hot Jupiter) given arbitrary molecular abundances (constant with altitude or variable with altitude), thermal structures, and cloud/aerosol properties (droplet sizes, single scatter albedo/asymmetry parameter, vertical distribution; Mai & Line 2019). The core radiative transfer scheme accounts for full multiple scattering of outgoing thermal radiation utilizing the methods outlined by Toon et al. (1989). We incorporate correlated-K ("resort-rebin"; Amundsen et al. 2017) opacities by generating precomputed, high-resolution cross section grids sourced from a variety of databases including ExoMol (Tennyson et al. 2016; Tennyson & Yurchenko 2018), utilizing the EXOCROSS routine (Yurchenko et al. 2018), and HITRAN/HITEMP (Rothman et al. 2010), via the HAPI routine (Kochanov et al. 2016). The transmission and emission routines have been validated on numerous occasions against other codes (Line et al. 2013a, 2013b; Morley et al. 2015) and used to analyze brown-dwarf observations (Line et al. 2014a, 2015, 2017).

The most significant change required to implement PIE into the standard CHIMERA emission spectrum forward model is to use the absolute flux from the system, F_{sys}. This differs from the standard emission spectroscopy approach, which models the wavelength-dependent secondary eclipse depth as the planet-to-star flux ratio, $\Delta F = F_p/F_s$. In this case, we define the system flux as the sum of all major flux sources in the exoplanetary system:

$$F_{\mathrm{sys}} = F_s + F_p + F_\epsilon, \qquad (1)$$

where F_s is the stellar flux, F_p is the planet flux, and F_ϵ is a catch-all term to account for any residual astrophysical flux source in the field (such as an additional, cooler planet or exozodiacal dust). For simplicity, we set $F_\epsilon = 0$ and focus on joint modeling of the stellar and planetary flux. We explore the ramifications of $F_\epsilon = F_{\mathrm{ez}}$ due to exozodiacal light in Section 3.4.

2.1.1. Planetary-flux Model

We use the standard CHIMERA emission-spectrum forward model presented by Line et al. (2013b, 2014b) and Batalha et al. (2018) with no modifications to the physics and chemistry. We employ the free chemistry (henceforth "free") forward model in our exploration of the PIE technique, which allows for the abundances of the gases in the state vector to take on any (physical, even if chemically implausible) values and assumes evenly mixed volume-mixing ratio vertical profiles. As such, we directly fit for the (log) gas abundances. Although we performed tests using the "chemically consistent" CHIMERA forward model (e.g., Kreidberg et al. 2015), which assumes thermochemical-equilibrium gas-vertical profiles, our results were generally consistent with those acquired with the "free" model and have been omitted for clarity and brevity.

For the temperature-pressure (TP) profile, we use the three-parameter, analytic radiative equilibrium model from Guillot (2010; see also Parmentier & Guillot 2014; Line et al. 2013b; Mai & Line 2019). The irradiation temperature T_{irr}, the infrared opacity $\log(\kappa_{\mathrm{IR}})$, and the single channel visible to IR opacity ratio $\log(g_1)$ are treated as free parameters, and the internal temperature T_{int} is fixed at 200 K.

Bringing together all of the physical, atmospheric, and thermal parameters that define our planet model, the planet flux is given as,

$$F_p = F_p(\theta_p) \qquad (2)$$

$$\theta_p = \{R_p, T_{\mathrm{irr}}, \log(\kappa_{\mathrm{IR}}), \log(g_1), \log(H_2O)$$
$$\times \log(CH_4), \log(CO), \log(CO_2), \log(NH_3)\}. \qquad (3)$$

2.1.2. Stellar-flux Model

We use Phoenix stellar models as the basis for our stellar-flux model (Allard et al. 2003, 2007, 2012). We access the stellar grids using the pysynphot code (STScI Development Team 2013) and linearly interpolate in effective temperature T_{eff}, surface gravity $\log(g)$, and metallicity $\log([M/H])$ between computed stellar models. We scale the stellar flux using the stellar distance, d, and stellar radius, R_s, so as to reproduce stellar-flux observations at Earth. This results in a five-parameter stellar-flux model that is parameterized via the following state vector,

$$F_s = F_s(\theta_s) \qquad (4)$$

$$\theta_s = \{T_{\mathrm{eff}}, \log(g), \log([M/H]), d, R_s\}. \qquad (5)$$

Table 1
Retrieved Constraints on WASP-43b using Multiple JWST Instruments to Simulate the PIE Technique

Parameters	Defaults	Priors	NIRISS SOSS (1 hr)	NIRSpec G395 (1 hr)	MIRI LRS (1 hr)	All (1 hr)	All (4 hr)
$T_{\rm eff}$	4305.0	$\mathcal{N}(4305, 174.75)$	± 0.020	± 0.065	± 0.16	± 0.018	± 0.0086
$\log([M/H])$	-0.05	$\mathcal{N}(-0.05, 0.17)$	± 0.000090	± 0.00080	± 0.0018	± 0.000069	± 0.000034
$\log(g)$	4.646	$\mathcal{N}(4.646, 0.052)$	± 0.000054	± 0.00031	± 0.00069	± 0.000050	± 0.000025
R_s	0.6629	$\mathcal{N}(0.6629, 0.0554)$	± 0.0025	± 0.0024	± 0.0025	± 0.0025	± 0.0025
d	86.7467	$\mathcal{N}(86.75, 0.33)$	± 0.33	± 0.32	± 0.32	± 0.32	± 0.33
R_p	0.93	$\mathcal{N}(0.93, 0.08)$	± 0.080	± 0.079	± 0.068	± 0.026	± 0.014
$T_{\rm irr}$	1000	$\mathcal{U}(300, 3000)$	± 100	± 105	± 303	± 41	± 20
$\log(\kappa_{\rm IR})$	-1.5	$\mathcal{U}(-3, 0)$	± 0.89	± 0.44	± 0.78	± 0.18	± 0.090
$\log(g_1)$	-0.7	$\mathcal{U}(-3, -1)$	± 1.0	± 0.83	± 1.1	± 0.18	± 0.044
H_2O	-3.0	$\mathcal{U}(-15, 0)$	± 5.1	± 1.7	± 2.3	± 0.39	± 0.16
CH_4	-8.0	$\mathcal{U}(-15, 0)$	± 4.9	± 3.6	± 5.1	± 3.1	± 3.0
CO	-7.0	$\mathcal{U}(-15, 0)$	± 5.0	± 4.7	± 5.1	± 3.7	± 3.3
CO_2	-8.0	$\mathcal{U}(-15, 0)$	± 4.6	± 3.5	± 5.0	± 2.9	± 2.7
NH_3	-10.0	$\mathcal{U}(-15, 0)$	± 5.1	± 3.8	± 5.3	± 3.5	± 3.2

Note. $\mathcal{U}$ denotes a uniform prior probability distribution described in terms of the lower and upper bounds, and $\mathcal{N}$ denotes a normal prior described by the mean and standard deviation.

2.1.3. Inverse Model

We use the emcee (Foreman-Mackey et al. 2013) implementation of the affine-invariant Markov Chain Monte Carlo (MCMC) ensemble sampler from Goodman & Weare (2010). For each simulation we set the number of walkers equal to 10 times the dimensionality of the model and randomly draw their initial positions from an estimate of the posterior variance obtained through Levenberg–Marquardt least-squares minimization (Moré 1978). We iteratively draw N samples until $N \gtrsim 50\tau$, where τ is the integrated autocorrelaion time. We performed a variety of tests using the dynesty nested-sampling algorithm (Skilling 2004; Speagle 2020), but found that it converged inefficiently due to the vast dynamic range in contribution to the likelihood between the stellar and planetary parameters. Therefore, our reported results were obtained exclusively using MCMC.

2.2. Synthetic JWST Observations

We use PandExo to simulate observations of WASP-43b with JWST (Batalha et al. 2017, 2018). PandExo uses the official JWST exposure-time calculator (ETC), Pandeia (Pontoppidan et al. 2016), to perform noise modeling for exoplanet observations. In this work, we focus exclusively on observations in the 0.6–12 μm wavelength range using NIRISS SOSS (Doyon et al. 2012), NIRSpec G395 (Ferruit et al. 2012), and MIRI LRS (Kendrew et al. 2015) because these instruments provide complete wavelength coverage over the stated range without saturating. We bin our simulated JWST data to a constant resolving power of $\mathcal{R} = 100$ for our retrieval analyses.

To study the efficacy of the PIE technique, we simulated high-resolution model spectra using the forward model described in Section 2.1 before implementing noise from PandExo. Furthermore, we do not add random Gaussian jitter to the data. Although these assumptions yield idealized observations that, by design, will be capable of being well fit by our nominal model, this exercise is common practice in the exoplanet retrieval literature (see Feng et al. 2018, for more details) and allows us to characterize bias and degeneracies in

the retrieval procedure, which are of keen interest in this study. Although we calculate the precision of our synthetic spectra using only PandExo noise calculations, we considered the effect of absolute flux calibration accuracy in the Appendix as it may complicate the study of broad wavelength spectra constructed using multiple instruments with offsets in absolute flux between them.

The first two columns of Table 1 provide the default choice of model parameters that were used to simulate the JWST observations. We used Gaia DR2 data for the stellar parameters (Gaia Collaboration et al. 2018; Bailer-Jones et al. 2018). For the planetary parameters, we used gas abundances and a TP profile that are consistent with the current estimates from retrievals of WASP-43b's transmission spectrum (Kreidberg et al. 2014). However, one notable departure from this convention is that we set the irradiation temperature ($T_{\rm irr}$) to 1000 K to be representative of the night side of this hot Jupiter (Beatty et al. 2019). The third column of Table 1 shows the Bayesian prior probability distributions used throughout this investigation, unless otherwise stated.

3. Results

Figure 1 shows a conceptual demonstration of the PIE technique. The top panel of Figure 1 depicts a model spectrum of the WASP-43 system, where the observed flux is a combination of the stellar ($\sim$4400 K) and planetary night-side ($\sim$1000 K) spectra. We include simulated 1σ uncertainties on the observed flux, corresponding to a 4 hr exposure with each JWST instrument mode considered, but the error bars are much smaller than the point size. As in Stevenson (2020), we show the PIE signal enhanced by a factor of $1000\times$ to aid in visualizing the contribution to the total system flux from the planet as a function of wavelength. However, we emphasize that this enhancement is not used in any part of the analysis. Crucially, the planet provides negligible flux compared to the star at short wavelengths near the peak of the stellar spectral energy distribution (SED), which yields a "reference wavelength range" that is optimal for constraining the stellar flux. The relative contribution from the planet to the total observed flux grows with wavelength, extending a lever arm with which
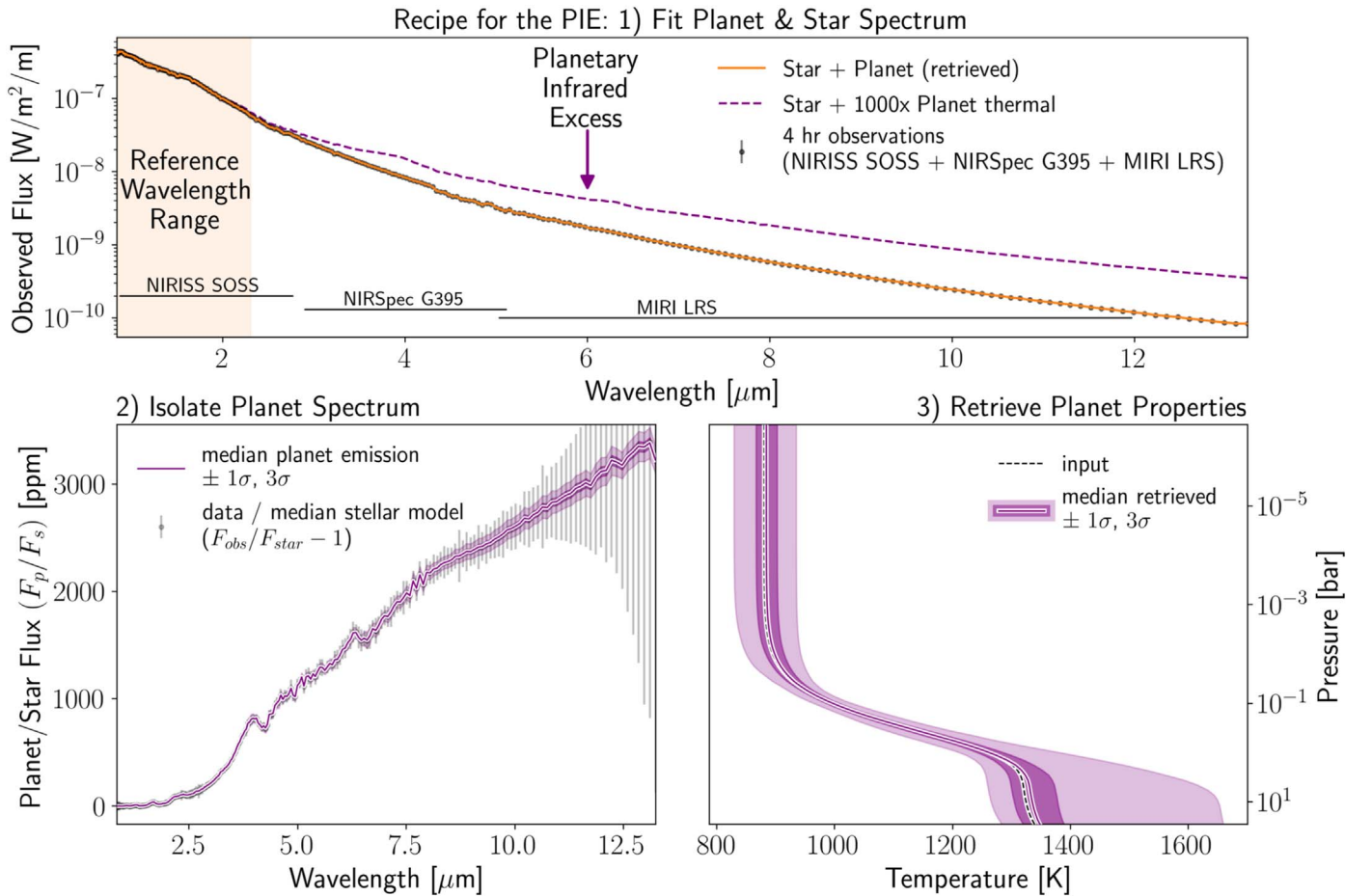
Figure 1. *Top:* figure depicting the concept of PIE for the WASP-43 planetary system. The observed stellar plus night-side planetary flux ($\sim$1000 K) is shown simulated across the JWST wavelength range, enabling a retrieval of WASP-43b's night-side atmospheric properties. The planet thermal emission is shown enhanced by a factor of 1000 K for visual clarity, although it is not enhanced in the lower panels or for the actual analysis. Using data from the reference wavelength range ($<$2.3 μm) to calibrate the stellar model, we can isolate and infer the planet's infrared excess by simultaneously fitting the stellar and planet spectra. *Lower left:* the planet's thermal emission is shown relative to the median retrieved stellar model with 1σ and 3σ credible regions. *Lower right:* retrieved constraints on WASP-43b's night-side temperature-pressure profile. There is no retrieved bias relative to the input TP profile.

to isolate and constrain the planet spectrum and atmospheric properties.

The lower panels of Figure 1 demonstrate how the PIE signal can be uniquely isolated when the stellar spectrum is properly accounted for (lower left panel), which allows the planet's emission spectrum to be fit using an atmospheric retrieval model and enables the inference of planetary atmospheric properties, such as the temperature structure (lower right panel). In this example, the broad wavelength coverage and high-precision simulated JWST observations permit a robust inference of the TP profile.

Figure 2 expands on the results of the retrieval shown in Figure 1 by showing the full 1D and 2D marginalized posterior distributions for the stellar and planetary parameters in the upper right corner and lower left corner, respectively. In general, posterior constraints on the stellar parameters are very tight. In practice, we anticipate that stellar spectral and temporal variability due to granulation, spots, and faculae will limit the precision of these inferred stellar parameters, but we discuss this further in Section 4. As expected, the stellar radius and distance to the system are mathematically degenerate and show Gaussian posteriors that are identical to their respective priors taken from Gaia. Although Figure 2 omits covariances

between stellar and planetary parameters, no such degeneracies were identified.

The planetary parameters are also quite well constrained. The irradiation temperature is inferred to about $\pm$20 K. The H2$_O$ abundance is retrieved to a precision of $\pm$0.16 dex. Although the abundances of CH_4, CO, CO_2, and NH_3 are not well constrained, we retrieve credible upper limits that are consistent with their respective low-abundance input values. The planet radius and irradiation temperature show a negative correlation analogous to the findings of S20 using simple blackbody models. Slight covariances are apparent between the parameters controlling the TP profile, but the TP profiles shown in Figure 1 calculated from posterior samples reveal an accurate picture of the input atmospheric thermal structure.

We used the Bayesian Information Criterion (BIC) to verify that the JWST quality data warrants the inclusion of the planetary-flux component in our retrievals. To compare against the results shown in Figures 1 and 2, we ran another retrieval on the simulated spectrum that omitted the planetary-flux model and all of the corresponding parameters. We found that this yielded a ΔBIC $\approx$ 40,000, favoring the model with components for the planet and star. This indicates that the fit to the spectrum is drastically improved by the addition of the planet model, which makes negligible the "Occam's razor"
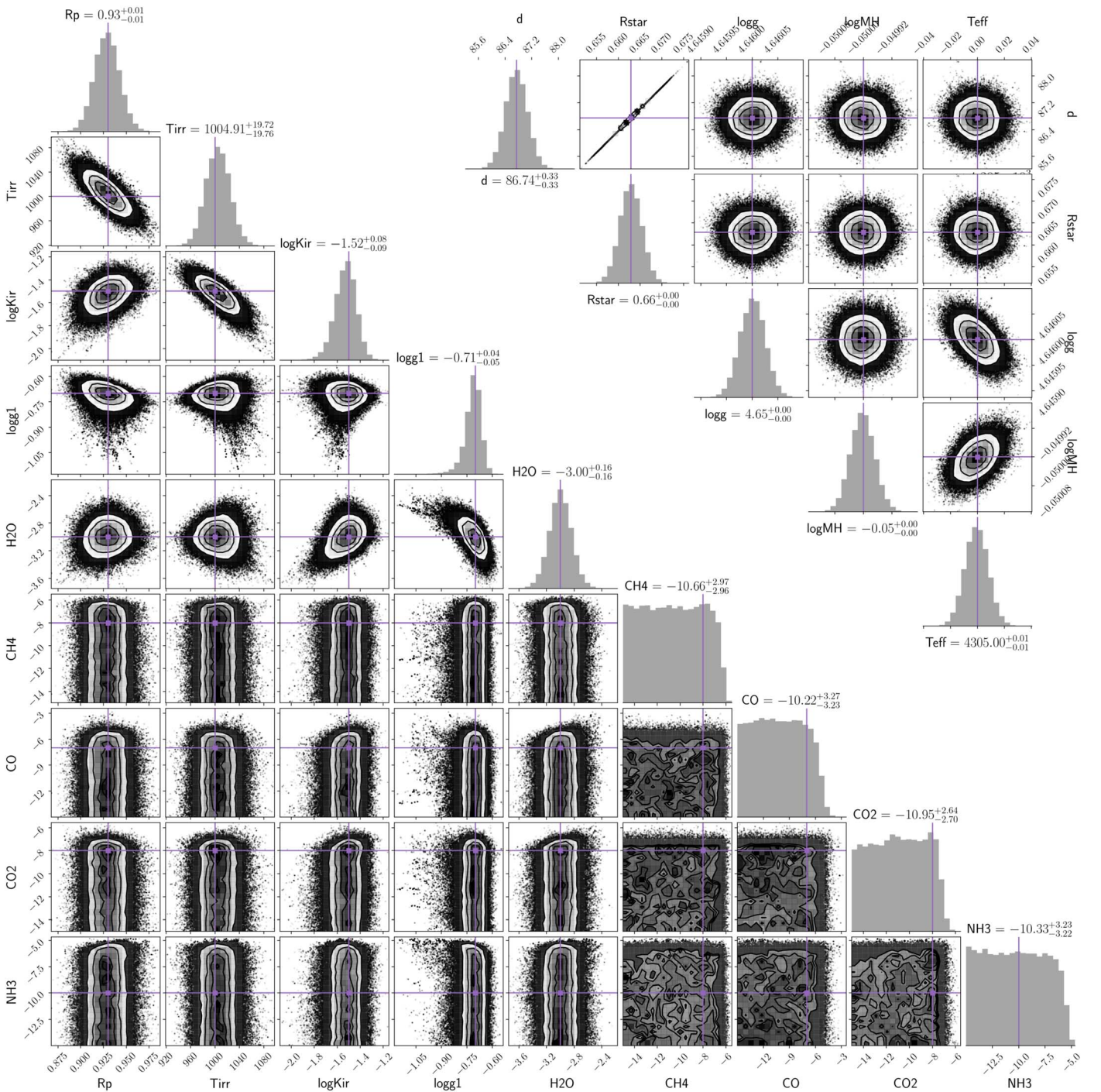
Figure 2. Corner plot showing the 1D and 2D marginalized posterior distributions for the stellar (upper right) and planetary (lower left) parameters from a PIE retrieval. These results used data and uncertainties simulated from 4 hr exposures with each of JWST's NIRISS SOSS, NIRSpec G395, and MIRI LRS instrument modes. We identify no significant correlations between the stellar and planetary parameters (covariances are not shown). Outside of the stellar radius/distance degeneracy, the stellar parameters are precisely constrained by the data. For WASP-43b, the data are sufficiently precise to constrain the planet radius, night-side thermal structure, and H_2O abundance. Additional telescope time is needed to adequately constrain the abundances of other prominent molecules.

penalty incurred on the BIC by nine additional free parameters. Thus, it may be possible to use this type of model comparison to accurately diagnose the presence of PIE using precise, broad wavelength stellar spectra.

In the following subsections we expand our investigation to consider wavelength range, non-transiting planets, exposure time, and exozodiacal light contamination.

3.1. Wavelength Range and JWST Instrument Selection

Our initial retrieval used simulated JWST data for 4 hr out-of-transit observations with NIRISS SOSS, NIRSpec G395, and MIRI LRS to achieve continuous wavelength coverage between 0.6 and 12 μm. Now we examine the result of using individual instruments. Table 1 shows our retrieval results where each column lists 1σ constraints on each retrieved model

parameter (rows) for multiple experiments using different JWST instrument modes (columns). Note that the final column on the right shows results for 4 hr with all three instruments and corresponds to the results shown in Figure 1 and Figure 2, while the other columns correspond to 1 hr exposures.

As expected, retrievals on the full wavelength range provide the best constraints on the stellar and planetary parameters, but the performance of individual instruments varies from parameter to parameter. For example, we find that shorter wavelength observations that resolve the peak of the stellar SED offer the best constraints on the stellar parameters, with the tightest constraints on the effective stellar temperature ($T_{\rm eff}$) provided by NIRISS, then NIRSpec, then MIRI. Similarly, the planet's 1000 K night-side emission peaks at 2.9 μm; therefore, its irradiation temperature ($T_{\rm irr}$) is best constrained by either NIRISS or NIRSpec, while MIRI offers a $3\times$ worse constraint. However, the planet radius (R_p) is essentially unconstrained by the individual use of NIRISS or NIRSpec (where the posteriors are consistent with the priors), but shows an improved posterior constraint using only MIRI data. Despite the lack of radius constraint from using NIRISS or NIRSpec on their own, the planet radius is significantly better constrained using data from all three instruments. This result is consistent with the presence of a correlation between planet radius and irradiation temperature shown in Figure 2, which we will revisit in Section 3.2 for non-transiting planets. Regarding constraints on H_2O, NIRSpec G395 provides the best individual constraint of ± 1.7 dex, MIRI LRS provides the next best constraint of ± 2.3 dex, and NIRISS SOSS is much worse at ± 5.1 dex. These abundance results that favor the use of NIRSpec reflect a combination of the rising sensitivity to the planet thermal emission with wavelength and the specific wavelengths that exhibit H_2O absorption features.

To examine how marginalizing over uncertainties in the stellar spectrum decreases the precision on retrieved planetary parameters when using the PIE technique, we ran a series of retrievals with the stellar flux fixed at the true input value. This simulates the traditional secondary eclipse retrieval approach. We kept the exposure time per instrument fixed at 4 hr and simulated individual cases for NIRISS, NIRSpec, and MIRI. Using a fixed stellar flux resulted in tighter constraints on, in particular, the planet's irradiation temperature and radius, with the largest effect seen toward longer wavelengths. When marginalizing over the stellar fit using the PIE technique we observed a $1.0\times$, $2.4\times$, and $3.5\times$ decrease in the precision on the retrieved irradiation temperature using NIRISS, NIRSpec, and MIRI, respectively, and a $1.1\times$, $2.3\times$, and $2.5\times$ decrease in the precision on the retrieved planet radius. We observed no decrease in the precision of molecular abundances. Thus, long wavelength PIE observations in the MIR that lack the NIR reference wavelength range to constrain the stellar spectrum suffer the greatest loss in precision of retrieved planetary information relative to traditional secondary eclipse measurements. One potential caveat that must be considered when applying the PIE technique to absolute fluxes is that JWST's absolute flux calibration accuracy may limit the ability to use the PIE technique on panchromatic spectra stitched together from observations using different JWST instruments with non-negligible offsets caused by their absolute flux calibration. We investigated this in detail in the Appendix and found that if JWST achieves its nominal requirement of 2% absolute flux calibration accuracy, offset-correction parameters can be used within the PIE retrieval to enable the analysis of spectra

obtained with different instruments. Using 2% offsets between instruments, we find that the retrieved molecular abundances in the planetary atmosphere are completely unaffected and a relatively small loss in precision (the 1σ uncertainties grow by $<50\%$) is incurred for the stellar radius, planetary radius, and irradiation temperature relative to the baseline results using all three instruments without calibration offsets (shown in Table 1). Even with 2% instrument offsets to simulate absolute flux calibration, our results indicate that using all three JWST instruments—NIRISS SOSS, NIRSpec G395, and MIRI LRS to observe near-continuous wavelength coverage between 0.6 and 12 μm still outperforms any single instrument for night-side characterization of WASP-43b with the PIE technique.

3.2. Transiting versus Non-transiting Planets

By using spectral information to separate planets from stars, the PIE technique offers an opportunity to study the thermal emission from non-transiting planets. For the purposes of this work, we assume that non-transiting planets have known orbits but an unknown radius, like those detected from radial-velocity (RV) surveys. However, we remain focused on a WASP-43b-like exoplanet. Instead of using the Gaussian prior on planet radius shown in Table 1 from transit observations, we use an uninformative uniform prior given by $\mathcal{U}(0.5, 1.5)$.

Figure 3 shows 1D and 2D marginalized posterior distributions for WASP-43b night-side PIE retrievals assuming no informative prior information about the planet radius. The 1D marginal posteriors show that, if only one instrument is used, planet temperature can be better constrained with shorter wavelength observations and planet radius can be better constrained at longer wavelengths. Both the planet radius and temperature can be much better constrained by combining data from two or three instruments. Using only two instruments, the irradiation temperature is best constrained with combined data from NIRISS and NIRSpec, while the planet radius is best constrained with NIRISS and MIRI. Intriguingly, the 2D posterior projection between irradiation temperature and planet radius shows how their covariance changes with each instrument.

3.3. Varying Exposure Time

Here we briefly consider the effect of varying the exposure time. We repeated our previous retrieval that used data from 1 hr exposures with all three JWST instrument modes, now using 0.25 hr and 4 hr exposures to halve and double the signal-to-noise ratio (SNR) of the data, respectively, compared to the fiducial case. Table 1 provides the constraints for the 1 hr and 4 hr cases. With the exception of prior-dominated parameters (e.g., the stellar radius and distance) and unconstrained parameters with non-Gaussian posteriors (e.g., CH_4, CO, etc.), our exposure-time experiment yielded results that scaled with SNR exactly as expected. For example, the 1σ constraint on the planet radius dropped (rose) from $\pm 0.026 \, R_J$ to $\pm 0.014 \, R_J$ ($\pm 0.051 \, R_J$), approximately a factor of 2, for a $2\times$ increase (decrease) in data SNR. We note that these tests do not include the effect of a noise floor in the observations, which may cause wavelength-dependent deviations in the scaling of SNR with the square root of the exposure time that could propagate through the parameter inference. The effects of various noise floors on PIE retrievals will be explored in an upcoming paper. Our 4 hr NIRISS SOSS spectrum reaches a
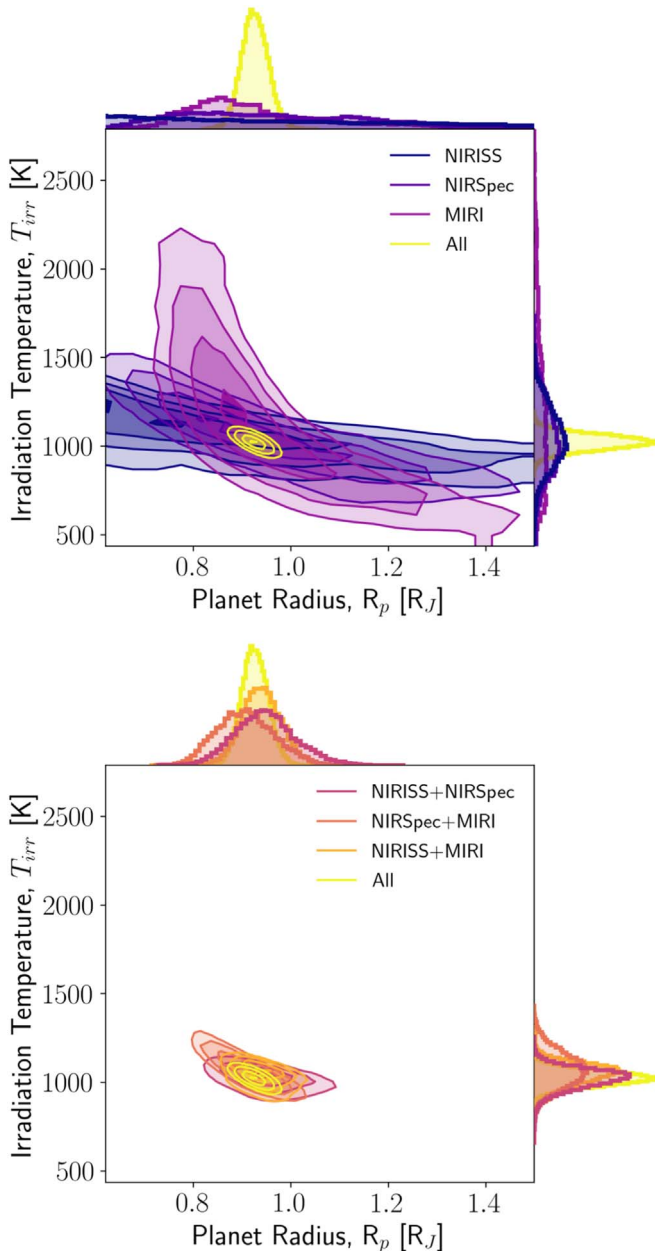
Figure 3. One- and two-dimensional marginalized posterior distributions for the retrieved irradiation temperature and radius of WASP-43b from synthetic night-side observations with JWST. Observations assume 1 hr exposures with each instrument given in the legend. The degeneracy between planet temperature and radius depends on the observed wavelength range and can be broken with sufficiently broad wavelength coverage due to the wavelength dependence (independence) of thermal emission on temperature (radius).

maximum precision of 17 ppm at 1.4 μm with $\mathcal{R} = 100$. While the exact wavelength coverage needed to precisely constrain the planet parameters will change with planet temperature, for the non-transiting exoplanet case we recommend maximizing the wavelength coverage instead of repeated observations with a specific instrument mode.

3.4. Sensitivity to Exozodiacal Dust

A key concern for the PIE technique is the presence of exozodiacal dust in exoplanetary systems and how the thermal emission from such dust may be incorrectly attributed to planetary thermal emission and could propagate biases into the

retrieval of atmospheric parameters. To estimate the magnitude of this effect within the context of our previous findings, we conducted a series of retrieval simulations with exozodiacal emission injected into the observed spectrum. We varied the intensity of the exozodiacal signal injected in the simulated data, but initially we did not attempt to retrieve the exozodiacal signal; instead we seek to characterize the bias that manifests in the inference if exozodiacal dust is not accounted for by the retrieval model.

We modeled exozodiacal flux (emitted and reflected) in the WASP-43 system using Zodipic (Kuchner 2012). We assumed the following properties for WASP-43, $R_* = 0.663 \, R_\odot$, $L_* = 0.136 \, L_\odot$, $T_* = 4305 \, \text{K}$, $d = 86.7467 \, \text{pc}$, $\log g = 4.492$, and solar metallicity. By default, the dust in the disk is considered to scatter isotropically and scattered light is only considered when $\lambda < 4.2 \, \mu$m. The inner spherical dust radius corresponds to a dust temperature of 1500 K, which is appropriate for removal from the system via sublimation in the absence of a planet. In reality, a planet could change the morphology of the disk and cause dust to collect at various mean-motion resonances and clear out annuli (Stark et al. 2013), but we assume the simple case of an isolated and smooth disk out to 3.28 au. We modeled the spectral contribution from 0.3 μm to 30 μm assuming a pixel size of 1 mas.

For this exozodiacal sensitivity study, we considered only the case with the highest quality data, which used all three JWST instruments to span 0.6–12 μm and assumed a 4 hr exposure time for each instrument mode. We tested adding 1 zodi, consistent with a solar system level of zodiacal dust, 3 zodis, consistent with the median zodi level for Sun-like stars (Ertel et al. 2020 found the median, $m = 3^{+6}_{-3}$), and 10 zodis.

We find that neglecting exozodiacal emission in PIE retrievals can bias the retrieved planet radius and, to a lesser extent, the planet temperature for systems with high exozodiacal levels. The left panel of Figure 4 shows the retrieved 1D and 2D marginalized posteriors for the planet radius and irradiation temperature for a set of simulations with varying exozodiacal contamination in the observed spectrum. For the case without exozodiacal contamination ($N_{\text{ez}} = 0$), we retrieve posteriors that are centered at the input value used to generate the JWST spectra. Increasing the exozodiacal contamination in the simulated system biases the retrieved planet radius to higher values in order to account for the additional system flux. This radius bias corresponds to 0.00558 R_J (~ 400 km) per zodi in the WASP-43 system. Similarly, the retrieved irradiation temperature shifts to lower values with increasing zodi, consistent with the anticorrelation seen between radius and temperature. We find that the bias in radius can be statistically significant with 1.1σ and 4.2σ radius increases for $N_{\text{ez}} = 3$ and $N_{\text{ez}} = 10$, respectively, but the corresponding bias in irradiation temperature is negligible ($<1\sigma$ for $N_{\text{ez}} = 10$) for this JWST test case. We note that for our high exozodiacal case with $N_{\text{ez}} = 10$, the stellar gravity $\log(g)$, TP profile parameter $\log(g_l)$, and H_2O abundance are all marginally biased by about 1σ.

As a final test of exozodiacal contamination, we incorporated a simple exozodiacal emission model into our PIE retrieval in order to explore the ability to mitigate the aforementioned biases. In this case, Equation (1) becomes

$$F_{\text{sys}} = F_s + F_p + F_{\text{ez}}, \qquad (6)$$
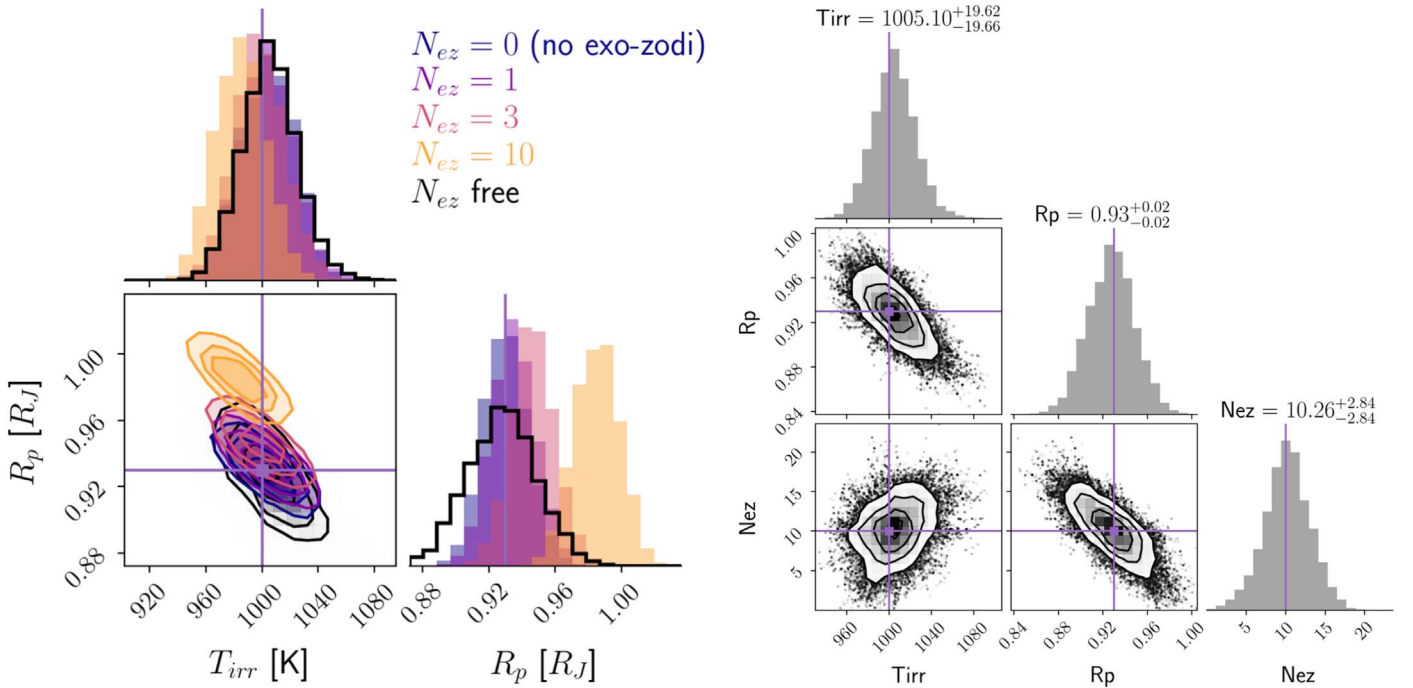
Figure 4. *Left:* one- and two-dimensional marginalized posterior distributions for the retrieved night-side irradiation temperature and radius of WASP-43b from synthetic JWST observations assuming four different levels of exozodiacal contamination. Failing to account for exozodiacal emission can bias the retrieved planet radius, and the planet's temperature to a lesser extent, particularly for systems with high exozodiacal levels. *Right:* marginalized posteriors for a PIE retrieval that explicitly fits for N_{ez}. The synthetic JWST data were generated with $N_{ez} = 10$. A subset of the total parameter space is shown to highlight the most affected parameters. Fitting for the zodi level removes the bias in planet parameters, but increases their uncertainties.

where F_{ez}—the exozodiacal spectrum—replaces F_ϵ. The exozodiacal light is assumed for simplicity to be dependent only on the level of exozodiacal dust in the system, N_{ez}, which linearly scales the fiducial spectrum. We then performed the same retrieval experiment as above with $N_{ez} = 10$ contamination, except with N_{ez} as an additional free parameter.

The right panel of Figure 4 shows the results of our exozodiacal retrieval for a subset of the free parameters that are most tied to the effects of exozodiacal emission. The zodi level in the system is constrained to $N_{ez} = 10.26 \pm 2.84$, which is consistent with our injected value. The covariance between planet radius and exozodiacal level shows a clear antic-orrelation, but no significant correlation is seen between zodi and irradiation temperature. Including N_{ez} as a free parameter successfully mitigates the radius bias; however, this comes at the cost of additional radius uncertainty due to the margin-alization over the zodi uncertainty propagated through the radius–zodi covariance. Compared to the case with no exozodiacal light ($N_{ez} = 0$), the planet radius uncertainty in this scenario grows by a factor of ∼1.5. Although we achieve a slightly better fit to the spectrum when we include N_{ez} as a free parameter, using the BIC for model selection marginally favors the model without N_{ez} (ΔBIC = 1.7) due to the penalty of adding another dimension to the inference. This suggests that it may be difficult, in practice, to confidently diagnose the presence of exozodiacal contamination and mitigate potential biases, but systems with even greater zodi or a different system configuration may not have this issue.

4. Discussion and Conclusion

We have developed a novel exoplanet atmospheric retrieval algorithm for use with the PIE technique that performs a joint fit to unresolved stellar and planetary spectra in the near to mid-IR. We used synthetic JWST observations of the hot Jupiter WASP-43b just outside of transit to explore the ability to use PIE to infer atmospheric characteristics of the planet's night side. Using a simple five-parameter stellar spectral model and a nine-parameter planetary model, we find that the stellar and planetary spectra can be uniquely constrained with no apparent degeneracies between their respective parameters. We also find that typical out-of-transit observation times (e.g., 1–4 hr) may be sufficient to constrain planet properties. Broad wavelength coverage with JWST using a combination of NIRISS, NIRSpec, and MIRI observations will greatly benefit the inference of planetary atmospheric parameters using the PIE technique as long as JWST meets its nominal 2% absolute flux calibration accuracy requirement.

For non-transiting planets without well-constrained radii, the planet radius and (irradiation) temperature are degenerate. However, we find that the morphology of the degeneracy depends on the wavelength range of the data relative to the peak of the planetary emission spectrum. As a result, the PIE technique appears capable of breaking the radius-temperature degeneracy and constraining both parameters if sufficiently broad wavelength coverage is available. While we have not considered the mass-inclination degeneracy that exists for RV planets (Hatzes 2016), the thermal signature of an exoplanet observed with the PIE technique, and its variability with time, will depend on orbital inclination and may enable it to be constrained. Furthermore, the radius constraints from PIE reported in this work could be combined with exoplanet mass–radius relationships to help break the mass-inclination degeneracy for RV planets. Future work will investigate the effects of unknown inclination on PIE.

We investigated the potential for exozodiacal emission from dust grains in exoplanet systems to compromise the PIE technique and subsequent planet inferences. We found that, indeed, strong ($N_{ez} \sim 10$) unresolved exozodiacal emission in observed systems can cause a significant bias in the retrieved planet radius, and to a lesser extent planet temperature, which could be significant for non-transiting planets in systems with above average exozodiacal levels if left unaccounted for. However, by implementing a simple exozodiacal model within our PIE retrieval framework, we demonstrated that the bias can be mitigated, at a small cost of planet radius precision, by fitting for the zodi emission.

4.1. Future Work

Although we have demonstrated that the PIE technique may be a viable strategy for thermal studies of transiting and non-transiting hot exoplanet atmospheres, more work will be needed to expand on our findings and to relax assumptions that we have made (e.g., static stellar and planetary-flux sources, single-planet chemical composition, no systematic noise, etc.). Most critically, we have assumed a simple stellar spectral model that does not account for stellar granulation, spots, or faculae, which will all add complexity to the stellar spectrum inference problem that must be solved for any planet information to be inferred. A more sophisticated stellar model with multiple spectral components for cool spots and hot faculae may cause degeneracies in the stellar fit that could decrease the precision on inferred stellar parameters from those found in this work. It remains unclear if these stellar complexities will be degenerate with the planetary spectrum and parameters since their temperatures differ sufficiently well to be separated. Additionally, we have considered only a WASP-43b-like planet with a $\sim$ 1000 K night side. The PIE technique will only increase in difficulty toward smaller and cooler planets that emit less flux. More work is needed across a broad range in planet and star temperatures to identify the optimal and plausible bounds for the PIE technique with JWST and other future mission concepts.

Finally, our exploration into exozodiacal contamination highlights how additional unresolved flux sources may confuse and bias the PIE technique. We showed that increasing the complexity of our PIE retrieval model to account for exozodiacal light did mitigate the bias, but in the same stroke decreased the precision of our inferred planet radius. This serves as a cautionary warning if too many unresolved sources and/or yet unidentified complicating effects enter the picture: the fidelity of planetary information could be lost to these degeneracies. These questions and others require additional study in order to advance the maturity of the PIE technique. Ultimately, our work has demonstrated that the out-of-transit baseline observations that are already planned with JWST for many hot Jupiters will provide an opportune test bed for night-side atmospheric characterization using the PIE technique.

Appendix
Absolute Flux Calibration Accuracy

To investigate the possible effects of absolute flux calibration on our PIE retrievals of spectra collected with different JWST instruments, we conducted an additional experiment with offsets between the NIRISS, NIRSpec, and MIRI data. Given that the nominal JWST requirement is 2% absolute flux-prediction accuracy for these instruments,[4] we generated synthetic observations using our 4 hr exposure experiment from Figures 1 and 2 with flux offsets imposed between the spectra of NIRISS, NIRSpec, and MIRI to misalign the panchromatic spectrum. We considered two different cases with 2% calibration offsets: "Case 1" with +2%, −2%, and +2% flux offsets for NIRISS, NIRSpec, and MIRI, respectively, and then we flipped the signs of the offsets for "Case 2" and used −2%, +2%, and −2%. To account for the absolute flux calibration in our retrieval, we added three flux offset parameters—one for each instrument—to allow the retrieval to fit for the proper offsets between the model spectrum and the data. We did not consider how slight overlaps in instrument wavelength range (e.g., between NIRSpec G395 and MIRI LRS) could be used as another means to correct for offsets due to calibration. We used uniform priors on the three flux-offset parameters of $\mathcal{U}(-0.05, +0.05)$ to keep them bounded within ±5%. We then ran three retrieval experiments, two using the Case 1 and Case 2 2% calibration-offset spectra and a third "Case 3" using the original data with 0% offsets to explore the impact of marginalizing over the three additional calibration parameters. Our results show that, in general, accounting for the 2% absolute flux prediction accuracy does reduce the retrieved precision on some of the stellar and planetary parameters, but the PIE method still yields reliable results that are a significant improvement over the results from any one instrument. Figure 5 shows a subset of the retrieval results for our three calibration-offset experiments compared against the baseline case with no instrument offsets and no offset-correction parameters. The stellar radius is the parameter most affected by the 2% offset cases, which yielded 50% and 40% larger retrieved uncertainties for Case 1 and Case 2, respectively, and is biased slightly high in Case 1. The stellar radius and distance degeneracy is shown in the right panel and appears significantly broadened for cases with offset corrections due to an anticorrelation between stellar radius and the offset parameters. The distance to the system is much less correlated with the offset parameters. The planet radius and irradiation temperature have 30%–40% larger uncertainties in these experiments, but the constraints on gas abundances are unaffected by our procedure to

---
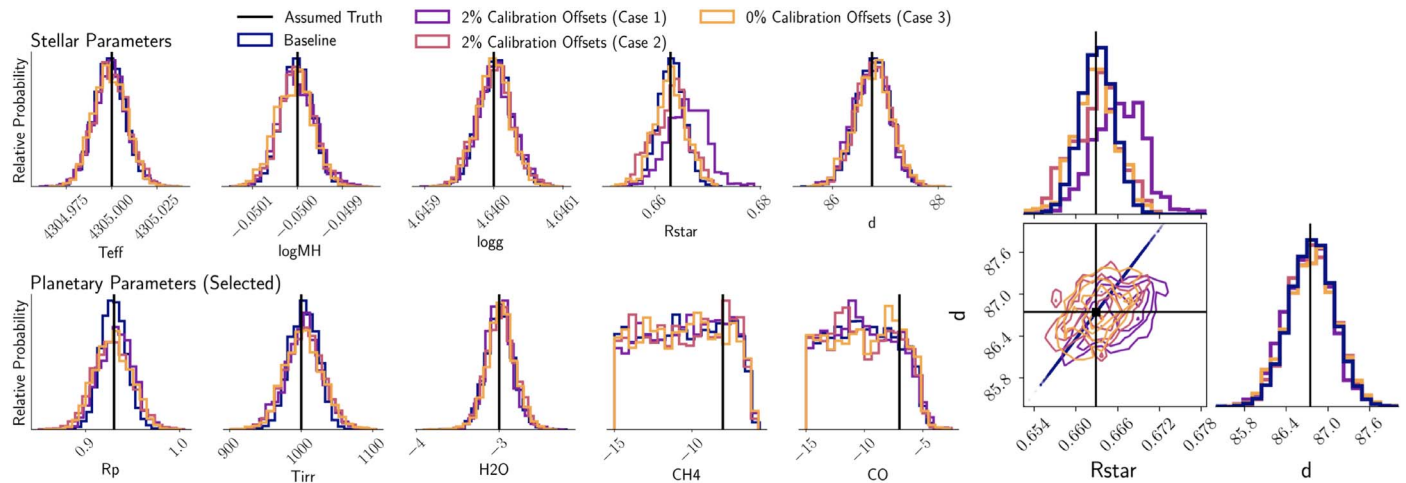
Figure 5. Posterior PDFs for a subset of the retrieved parameters for our investigation into absolute flux calibration offsets between JWST instruments compared against the assumed input values (black lines) and baseline retrieval analysis. The top row of panels shows the stellar parameters, the bottom row shows a selection of the planetary parameters, and the 2D contour on the right shows how the positive correlation between distance and stellar radius is broadened when instrument offset parameters are included in the PIE retrievals.

account for absolute flux calibration. These results indicate that if JWST achieves its nominal requirement of 2% absolute flux calibration accuracy, the PIE technique will be capable of analyzing spectra obtained with different instruments with offsets between them, incurring a relatively small (<50%) loss in precision for some retrieved planetary parameters.

ORCID iDs

Jacob Lustig-Yaeger ◉ https://orcid.org/0000-0002-0746-1980
Kevin B. Stevenson ◉ https://orcid.org/0000-0002-7352-7941
L. C. Mayorga ◉ https://orcid.org/0000-0002-4321-4581
Kristin Showalter Sotzen ◉ https://orcid.org/0000-0001-7393-2368
Erin M. May ◉ https://orcid.org/0000-0002-2739-1465
Noam R. Izenberg ◉ https://orcid.org/0000-0003-1629-6478
Kathleen Mandt ◉ https://orcid.org/0000-0001-8397-3315

References

Allard, F., Allard, N. F., Homeier, D., et al. 2007, A&A, 474, L21
Allard, F., Guillot, T., Ludwig, H.-G., et al. 2003, in Symposium-International Astronomical Union: Model Atmospheres and Spectra: The Role of Dust, 211, ed. E. Martín (Cambridge: Cambridge Univ. Press), 325
Allard, F., Homeier, D., & Freytag, B. 2012, RSPTA, 370, 2765
Amundsen, D. S., Tremblin, P., Manners, J., Baraffe, I., & Mayne, N. J. 2017, A&A, 598, A97
Arcangeli, J., Désert, J. M., Parmentier, V., Tsai, S. M., & Stevenson, K. B. 2021, A&A, 646, A94
Astropy Collaboration, Robitaille, T. P., Tollerud, E. J., et al. 2013, A&A, 558, A33
Bailer-Jones, C. A. L., Rybizki, J., Fouesneau, M., Mantelet, G., & Andrae, R. 2018, AJ, 156, 58
Batalha, N., Stevenson, K., Hill, M., et al. 2018, Natashabatalha/Pandexo: Starting Pandexo Releases v1.1.2, Zenodo doi:10.5281/zenodo.1256955
Batalha, N. E., Lewis, N. K., Line, M. R., Valenti, J., & Stevenson, K. 2018, ApJL, 856, L34
Batalha, N. E., Mandell, A., Pontoppidan, K., et al. 2017, PASP, 129, 064501
Beatty, T. G., Marley, M. S., Gaudi, B. S., et al. 2019, AJ, 158, 166
Beichman, C., Benneke, B., Knutson, H., et al. 2014, PASP, 126, 1134
Doyon, R., Hutchings, J. B., Beaulieu, M., et al. 2012, Proc. SPIE, 8442, 84422R
Ertel, S., Defrère, D., Hinz, P., et al. 2020, AJ, 159, 177
Feng, Y. K., Robinson, T. D., Fortney, J. J., et al. 2018, AJ, 155, 200
Ferruit, P., Bagnasco, G., Barho, R., et al. 2012, Proc. SPIE, 8442, 84422O
Foreman-Mackey, D. 2016, JOSS, 1, 24
Foreman-Mackey, D., Hogg, D. W., Lang, D., & Goodman, J. 2013, PASP, 125, 306
Gaia Collaboration, Brown, A. G. A., Vallenari, A., et al. 2018, A&A, 616, A1
Gardner, J. P., Mather, J. C., Clampin, M., et al. 2006, SSRv, 123, 485
Goodman, J., & Weare, J. 2010, Comm App Math Comp Sci, 5, 65
Guillot, T. 2010, A&A, 520, A27
Hatzes, A. P. 2016, in Methods of Detecting Exoplanets, Astrophysics and Space Science Library: The Radial Velocity Method for the Detection of Exoplanets, 428, ed. V. Bozza, L. Mancini, & A. Sozzetti (Cham: Springer), 3
Hunter, J. D. 2007, CSE, 9, 90
Kalirai, J. 2018, ConPh, 59, 251
Kendrew, S., Scheithauer, S., Bouchet, P., et al. 2015, PASP, 127, 953
Kochanov, R. V., Gordon, I., Rothman, L., et al. 2016, JQSRT, 177, 15
Kreidberg, L., Bean, J. L., Désert, J.-M., et al. 2014, Natur, 505, 69
Kreidberg, L., Line, M. R., Bean, J. L., et al. 2015, ApJ, 814, 66
Kuchner, M. 2012, ZODIPIC: Zodiacal Cloud Image Synthesis, Astrophysics Source Code Library, ascl:1202.002
Line, M. R., Fortney, J. J., Marley, M. S., & Sorahana, S. 2014a, ApJ, 793, 33
Line, M. R., Knutson, H., Deming, D., Wilkins, A., & Desert, J.-M. 2013a, ApJ, 778, 183
Line, M. R., Knutson, H., Wolf, A. S., & Yung, Y. L. 2014b, ApJ, 783, 70
Line, M. R., Teske, J., Burningham, B., Fortney, J. J., & Marley, M. S. 2015, ApJ, 807, 183
Line, M. R., Wolf, A. S., Zhang, X., et al. 2013b, ApJ, 775, 137
Line, M. R., Marley, M. S., Liu, M. C., et al. 2017, ApJ, 848, 83
Mai, C., & Line, M. R. 2019, ApJ, 883, 144
McKinney, W. 2010, in Proc. 9th Python Sci. Conf.: Data Structures for Statistical Computing in Python, ed. S. van der Walt & J. Millman (Austin, TX: SciPy), 56
Moré, J. J. 1978, in Numerical analysis Lecture Notes in Mathematics, 630 (Berlin: Springer), 105
Morley, C. V., Fortney, J. J., Marley, M. S., et al. 2015, ApJ, 815, 110
Parmentier, V., & Guillot, T. 2014, A&A, 562, A133
Pontoppidan, K. M., Pickering, T. E., Laidler, V. G., et al. 2016, Proc. SPIE, 9910, 991016
Price-Whelan, A. M., Sipőcz, B. M., Günther, H. M., et al. 2018, AJ, 156, 123
Rothman, L. S., Gordon, I. E., Barber, R. J., et al. 2010, JQSRT, 111, 2139
Skilling, J. 2004, in AIP Conf. Ser., 735, Bayesian Inference and Maximum Entropy Methods in Science and Engineering: 24th Int. Workshop on Bayesian Inference and Maximum Entropy Methods in Science and Engineering, ed. R. Fischer, R. Preuss, & U. V. Toussaint (Melville, NY: AIP), 395
Speagle, J. S. 2020, MNRAS, 493, 3132
Stark, C. C., Boss, A. P., Weinberger, A. J., et al. 2013, ApJ, 764, 195
Stevenson, K. B. 2020, ApJL, 898, L35

Stevenson, K. B., & Fowler, J. 2019, Analyzing Eight Years of Transiting Exoplanet Observations Using WFC3's Spatial Scan Monitor, Space Telescope WFC Instrument Science Report, arXiv:1910.02073

STScI Development Team 2013, pysynphot: Synthetic photometry software package, Astrophysics Source Code Library, ascl:1303.023

Tennyson, J., & Yurchenko, S. 2018, Atoms, 6, 26

Tennyson, J., Yurchenko, S. N., Al-Refaie, A. F., et al. 2016, JMoSp, 327, 73

Toon, O. B., McKay, C. P., Ackerman, T. P., & Santhanam, K. 1989, JGR, 94, 16287

van der Walt, S., Colbert, S. C., & Varoquaux, G. 2011, CSE, 13, 22

Virtanen, P., Gommers, R., Oliphant, T. E., et al. 2020, NatMe, 17, 261

Yurchenko, S. N., Al-Refaie, A. F., & Tennyson, J. 2018, A&A, 614, A131